

PROPER MOTIONS OF YOUNG STELLAR OUTFLOWS IN THE MID-INFRARED WITH SPITZER. II. HH 377/CEP E

NORIEGA-CRESPO, A.^{1,3}, RAGA, A. C.², MORO-MARTÍN, A.³, FLAGEY, N.^{4,6}, AND CAREY, S. J.⁵

Submitted 2013 November 27; accepted 2014 July 21

ABSTRACT

We have used multiple mid-infrared observations at 4.5 μm obtained with the Infrared Array Camera, of the compact (~ 1.4) young stellar bipolar outflow Cep E to measure the proper motion of its brightest condensations. The images span a period of ~ 6 yr and have been reprocessed to achieve a higher angular resolution ($\sim 0.8''$) than their normal beam ($\sim 2''$).

We found that for a distance of 730 pc, the tangential velocities of the North and South outflow lobes are 62 ± 29 and 94 ± 26 km s^{-1} respectively, and moving away from the central source roughly along the major axis of the flow. A simple 3D hydrodynamical simulation of the H_2 gas in a precessing outflow supports this idea. Observations and model confirm that the molecular Hydrogen gas, traced by the pure rotational transitions, moves at highly supersonic velocities without being dissociated. This suggests either a very efficient mechanism to reform H_2 molecules along these shocks or the presence of some other mechanism (e.g. strong magnetic field) that shields the H_2 gas.

Subject headings: circumstellar matter — stars: formation — ISM: jets and outflows — infrared: ISM — Herbig-Haro objects — ISM: individual objects (HH377/CepE)

1. INTRODUCTION

The measurement of proper motions for Herbig-Haro outflows and stellar jets has a long tradition and has played a fundamental role in our understanding of early phases of evolution of low mass stars, including their accretion rates, mass loss and disk dissipation (see e.g. McKee & Ostriker 2007; Bally 2009). The original work by Herbig & Jones (1981) on the first and brightest Herbig-Haro (HH) objects 1, 2 and 3, using photographic plates over a 34 yr period, set up the framework of the mass loss process in proto-stars and their interaction with the surrounding medium. The “knots” of HH 1 and 2 were found to have tangential velocities ranging from 100 to 350 km s^{-1} , in disagreement with the spectroscopic measurements that indicated that their emission was due to shocks of at most 100 km s^{-1} (see e.g. Raymond 1979). Modern observations and models have shown that HH 1 and 2 are the leading working surfaces or ‘bowshocks’ of highly collimated jet/counter-jet system that arises from a deeply embedded protostellar source of Class 0. And that a time dependent ejection can account for both larger proper motion and relative smaller shock velocities between their knots (see e.g. Raga et al. 2011a for a review). At optical wavelengths, using narrow band images at some of the brightest collisionally excited emission lines (e.g. $\text{H}\alpha$ and/or $[\text{SII}]$), it has been possible to measure proper motions for ~ 50 Herbig-Haro flows,

within a distance of roughly one kiloparsec, both from the ground and space (see e.g. Bally, Reipurth & Davis 2007; Caratti o Garatti & Eislöffel 2009) and over relative short periods of time (≤ 10 –20 yr). In the case of objects like HH 1/2, 34 and 46/47, such measurements have led to some spectacular time sequences of the outflows (see e.g. Hartigan et al. 2011). Proper motions are still a fundamental tool to find and correlate outflows across the sky and over distance scales of parsecs (see e.g. Reipurth et al. 2013). This method is particularly important when the outflow driving source has not been clearly identified. Radio observations have also been very successful in measuring proper motions of outflows for low and high mass protostars, taking advantage of the gas flow thermal (free-free) emission and high angular resolution measurements obtained by interferometric observations (see e.g. Rodriguez 2011).

At infrared wavelengths, however, it has been more difficult to measure proper motions because the lack of large format arrays. It has been until recently that near/mid-IR arrays have had a wide enough FOV to include a reasonable number of reference stars and be able to cross-correlate multiple epoch observations to derive the proper motions. The large proper motions observed in HH 1/2 system in the atomic ionic gas (Herbig & Jones 1981) have been measured in the NIR as well, using the molecular Hydrogen shock excited emission vibrational transition ($v=1-0$ S(1)) at 2.121 μm (Noriega-Crespo et al. 1997). It is now possible, using similar tracers, to measure the motions of multiple H_2 features in Cha II (Caratti o Garatti et al. 2009) or ρ Oph clouds (Zhang et al. 2013), with a similar range of transversal velocities (from 30 to 120 km s^{-1}).

In the mid-IR, thanks to the stability and longevity of the Infrared Array Camera (IRAC; Fazio et al. 2004) on board the Spitzer Space Telescope, it has been possible to measure the proper motions of several outflows in NGC1333 at an angular resolution of $2''$ (Raga et al.

¹ Infrared Processing and Analysis Center, California Institute of Technology, CA, 91125, USA

² Instituto de Ciencias Nucleares, Universidad Nacional Autónoma de México, Ap. 70-543, 04510 D.F., México

³ Space Telescope Science Institute, 3700 San Martin Dr., Baltimore, MD, 21218, USA

⁴ Jet Propulsion Laboratory, California Institute of Technology, CA, 91099, USA

⁵ Spitzer Science Center, California Institute of Technology, CA, 91125, USA

⁶ Institute for Astronomy, 640 North Aohoku Place, Hilo, HI, 96720, USA

2013; Paper I). IRAC channel 2 at $4.5 \mu\text{m}$ is an excellent tracer of the H_2 rotational emission, since three of the brightest lines, 0-0 S(11) 4.18, 0-0 S(10) 4.40 and 0-0 S(9) 4.18 μm fall within its passband (Noriega-Crespo et al. 2004a,b; Looney et al. 2007; Tobin et al. 2007; Ybarra & Lada 2009; Raga et al. 2011a, 2012; Noriega-Crespo & Raga 2012).

Using images obtained at $4.5 \mu\text{m}$ over a period of ~ 7 yr, Raga et al. (2013) obtained tangential velocities ranging from ~ 10 to 100 km s^{-1} (for a 220 pc distance) for 8 outflows in NGC 1333 cloud. For the bright HH 7-11 system, that lies at the center of the cloud, the H_2 tangential velocities of $\sim 10\text{--}15 \text{ km s}^{-1}$ are very close to those obtained at optical wavelengths using atomic gas line tracers, such as [SII] 6717/31Å or $\text{H}\alpha$ (Herbig & Jones 1983; Noriega-Crespo & Garnavich 2001).

In summary, proper motions, and the corresponding tangential velocities, are essential for determining the dynamics of the outflows, plus their momentum and energy transfer into the surrounding interstellar medium (see e.g. Quillen et al. 2005; Padoan et al. 2009; Plunkett et al. 2013). The striking morphological similarity between the atomic/ionic gas emission (obtained from optical or near-IR observations) and that of the molecular Hydrogen (obtained either from near/mid-IR observations), suggests that the kinematics of the protostellar outflows allow this relatively fragile molecule (H_2) either to survive the shocks or to regenerate itself rapidly in the dense postshock regions (see e.g. Le Bourlot et al. 2002; Panoglou et al. 2012). These issues can be partially addressed with studies of proper motions of the H_2 emission from stellar outflows.

In this study we determine the proper motions of the deeply embedded and compact molecular outflow Cep E, driven by a intermediate mass class 0 protostar (Eisloffel et al. 1996; Lefloch, Eisloffel & Lazareff 1996; Ladd & Hodapp 1997; Noriega-Crespo, Garnavich & Molinari 1998; Hatchel, Fuller & Ladd 1999; Moro-Martín et al. 2001; Noriega-Crespo et al. 2004b). Cep E is considered an excellent prototype of its kind, and therefore, has prompted many recent observations at millimeter and sub-millimeter wavelengths to study its H_2O and CO molecular content (Lefloch et al. 2011; Gómez-Ruiz et al. 2012; Tafalla et al. 2013), in part because its shocked excited South lobe is detected at optical wavelengths (HH 377; (Ayala et al. 2000).

At a distance of ~ 730 pc to Cep E, measuring proper motions with a time interval of ~ 6 yr (covered by the available IRAC images) is a considerable challenge, since velocities of $\sim 100 \text{ km s}^{-1}$ would correspond to shifts of only $\sim 0.17''$. In order to achieve as high a resolution as possible, we have employed a high angular resolution enhancement of the IRAC images, reaching a resolution of $0.6''\text{--}0.8''$ (see Velusamy, Langer & Marsh 2007; Velusamy et al. 2008; Noriega-Crespo & Raga 2012; Velusamy, Langer & Thomson 2014). Such an enhancement has recently been successfully applied to IRAC images of Cep E (Velusamy et al. 2011). Finally, given that observationally there is a tremendous morphological similarity between the mid-IR and NIR emission (Noriega-Crespo et al. 2004b), we expand the study to include some ground based H_2 2.12 μm NIR data that allows us to extend the time baseline of the observations

Table 1
Cep E Observations

Program ID	Request Key	Observing Date	Mean Coverage	t_{exp} (sec)	Observer
...	...	1996-08-22	...	1800.	Noriega-Crespo ^a
1063	6064384	2003-11-26	9	93.6	Noriega-Crespo ^b
20403	15571968	2005-12-25	4	41.6	Pipher ^b
20403	15570432	2006-08-09	4	41.6	Pipher ^b
60020	38734592	2010-02-01	8	83.2	Whitney ^{b,c}
...	...	2012-08-29	...	1500.	Flagey+
...	Noriega-Crespo ^a

^a Ground based 2.12 μm

^b IRAC 4.5 μm

^c Warm Spitzer Observation

to ~ 16 yr (Table 1).

The paper is organized as follows. The observations and their high angular resolution reprocessing is described in § 2. The determination of the proper motions is described in § 3. Finally, § 4 presents a summary of the results.

2. OBSERVATIONS & HIGH ANGULAR RESOLUTION REPROCESSING

The Cep E outflow was one of the first young stellar outflows observed with the Spitzer Space Telescope as part of their Early Release Observations (ERO; PID 1063, P.I. Noriega-Crespo) because of its strong brightness at mid-IR wavelengths. Its emission in the mid-IR ($5\text{--}17 \mu\text{m}$) is due mostly to bright H_2 rotational lines clearly detected already by the Infrared Space Observatory (ISO) with the infrared camera (ISOCAM) using its Circular Variable Mode (CVF; see e.g. Boulanger et al. 2005) that provided a low spectral ($R \sim 45$) and angular ($\text{FWHM} \sim 6''$) resolution spectral map of the region (Moro-Martín et al. 2001). The outflow was later observed by two ambitious programs, one to map the Cepheus OB3 molecular cloud to study its star formation (PID 20403, P.I. Pipher), and more recently by the GLIMPSE360 survey during the Warm Spitzer phase as one of the large Exploration programs (PID 60020, P.I. Whitney). The data, consisting of the basic calibrated frames or BCDs, have been recovered from the Spitzer Legacy Archive, version S18.18.0 (Cryo) and S19.0.0 (Warm). In all cases, the data was collected using the High-Dynamic-Range (HDR) mode with a 12 s integration time for the 'long' frames (10.4 s on target) and 0.6 s for the 'short' ones. A summary of the observations is presented in Table 1.

The BCDs were then reprocessed with the HiREs deconvolution software AWAIC³ (A WISE Astronomical Image Co-Adder), developed by the Wide Field Infrared Survey Explorer (WISE) for the creation of their Atlas images (see e.g. Masci & Fowler 2009; Jarrett et al. 2012). The AWAIC software optimizes the coaddition of individual frames by making use of the Point Response Function (PRF) as an interpolation kernel, to avoid flux losses in undersampled arrays like those of IRAC, and also allows a resolution enhancement (HiRes) of the final image, by removing its effect from the data in the

³ <http://wise2.ipac.caltech.edu/staff/fmasci/awaicpub.html>

deconvolution process. We have used this method quite successfully in the HH 1/2 outflow (Noriega-Crespo & Raga 2012), and as mentioned above, a similar method has been used on Cep E (Velusamy et al. 2011) and HH 46/47 (Velusamy et al. 2007). On IRAC images, the HiRes enhances the angular resolution from the standard $\sim 2''$ to $\sim 0.6''$ – $0.8''$ (Velusamy et al. 2008; Noriega-Crespo & Raga 2012).

The combination of being deeply embedded and its youth, ~ 5000 yr (Ladd & Hodapp 1997), perhaps makes Cep E one of the outflows where the morphology of the vibrational H_2 is nearly identical to the H_2 rotational emission observed with IRAC at $4.5 \mu\text{m}$. This similarity has encouraged us to introduce an earlier H_2 $v=1-0$ $2.12 \mu\text{m}$ image from 1996 and one recently obtained in 2012, in the analysis of the proper motions, providing a ~ 16 yr time baseline. The NIR 1996 image was obtained with the 3.5 m telescope at the Apache Point Observatory with a 256×256 array at $f/5$ and a 0.482 pixel^{-1} scale using a $2.12 \mu\text{m}$ filter (1% width) and $2.22 \mu\text{m}$ (4% width) to subtract the continuum. The complete analysis of these data was already presented by Ayala et al. (2000). The 2012 image was obtained at Palomar Observatory with the Wide Field Infrared Camera (WIRC) mounted in the 200in prime focus using a 2048×2048 Hawaii-II HgCdTe detector. WIRC has a field-of-view of $8.7'$ and a $0.2487 \text{ arcsec/pixel}$ scale (Wilson et al. 2003). The observations were carried out on August 29, 2012 in the $2.12 \mu\text{m}$ and K-continuum ($2.27 \mu\text{m}$, 2%) filters, with a 25 min total integration time. Figure 1 shows a comparison of the Palomar $2.12 \mu\text{m}$ continuum subtracted image with that at $4.5 \mu\text{m}$ from Noriega-Crespo et al. (2004b). Among some of the small obvious differences are the lack of H_2 vibrational emission on the same region where there is a “wide angle” cone at $4.5 \mu\text{m}$ (Velusamy et al. 2011), that strongly suggest to be scattered light by small dust particles; and the emission at $2.12 \mu\text{m}$ on the South lobe that fits within these “cones” and reaches further into the IRAS 23011+6126 central source. Other than these differences, the knots that we have used in our proper motion ‘boxes’ are indistinguishable from each other. In Figure 2 we show the five epochs that are being analyzed; the IRAC images are the HiRES AWAIC reprocessed after 60 iterations.

3. PROPER MOTION MEASUREMENTS

As can be seen in Figure 2, the Cep E outflow shows bipolar “cavity” structures which extend out to ~ 10 – $15''$ from the source (with an approximately NNE-SSW orientation). These cavities have two ridges that first open out from the outflow source, and then converge into compact emission structures. Further away ($\sim 20''$ from the source), we find two bow-like prolongations of the outflow lobes. As can be seen in Figure 2, the emission along the two-ridged cavities shows a complex time-dependence, with the Northern cavity becoming fainter and the Southern cavity brightening from 2003 to 2010 (i.e., the period covered by the IRAC images).

We have defined four boxes, including the regions of convergence of the cavities and the bow-like structures, which we show in Figure 4. For each of these four boxes, we have carried out cross correlations between the emission in the 2003.89 frame (the first of the IRAC frames, see Table 1) and the other 4 available frames. From

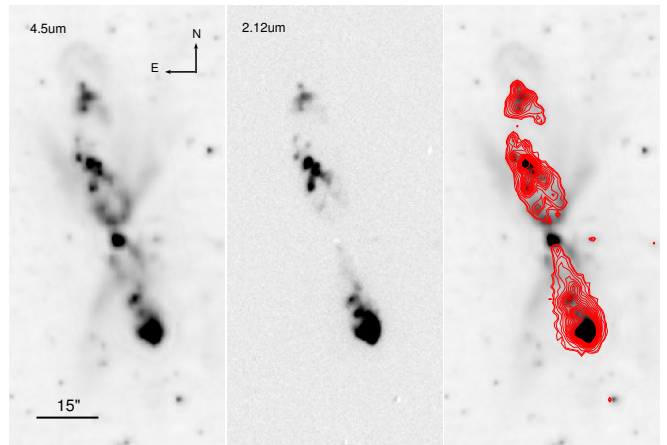


Figure 1. A comparison of the rotational H_2 emission as detected by IRAC at $4.5 \mu\text{m}$ in 2003.89 (left and right panels) with that from ground based observation of the vibrational H_2 $v = 1-0$ at $2.12 \mu\text{m}$ (central panel and red contours on the IRAC $4.5 \mu\text{m}$ image) obtained in 2012.66. From this comparison it looks that the $4.5 \mu\text{m}$ image includes in its cavity a significant component of continuum emission due to dust scattered light.

Table 2
Cep E Proper Motions and Tangential Velocities from
 $2.12 \mu\text{m}$ images^a

Box	Δ_x ^b mas/yr	Δ_y ^b mas/yr	V_x ^b km s ⁻¹	V_y ^b km s ⁻¹	V_T km s ⁻¹
1	4.0	-8.7	13.9	-30.2	33.0 ± 14.6
2	0.9	-2.6	3.1	-9.0	9.5 ± 14.0
3	-0.6	6.7	-2.1	23.3	23.4 ± 11.9
4	0.2	12.2	0.7	42.4	42.4 ± 11.2

^a For a distance of 730 pc

^b The proper motions have estimated errors of 3.2 mas/yr (11 km s⁻¹)

Table 3
Cep E Proper Motions and Tangential Velocities from IRAC
 $4.5 \mu\text{m}$ images^a

Box	Δ_x mas/yr	Δ_y mas/yr	V_x km s ⁻¹	V_y km s ⁻¹	V_T km s ⁻¹
1	14.7 ± 9.3	-10.4 ± 1.6	51.1 ± 32.3	-36.2 ± 5.6	62.6 ± 29.5
2	10.0 ± 1.4	-7.3 ± 6.8	34.8 ± 4.9	-25.4 ± 23.6	43.1 ± 17.9
3	2.7 ± 2.9	20.4 ± 8.1	9.4 ± 10.1	70.9 ± 28.2	71.5 ± 29.3
4	-12.8 ± 6.0	23.8 ± 5.4	-44.5 ± 20.9	82.8 ± 18.8	94.0 ± 26.5

^a For a distance of 730 pc

paraboloidal fits to the peak of cross correlation functions we then determine the offsets of the emission (within the four boxes, see Figure 4) with respect to the 2003.89 frame. For the two $2.12 \mu\text{m}$ images, we performed the cross correlation initially with 2003.89 frame as well, and then between themselves. In this way the offsets at 2.12 & $4.5 \mu\text{m}$ are measured on a common reference frame.

The resulting RA and DEC displacements for the four selected boxes are plotted as a function of time in Figure 3, where the stars and plus signs correspond to the 2.12 & $4.5 \mu\text{m}$ frames respectively. From this Figure, one notices that boxes 1 and 4 (corresponding to the bow-like

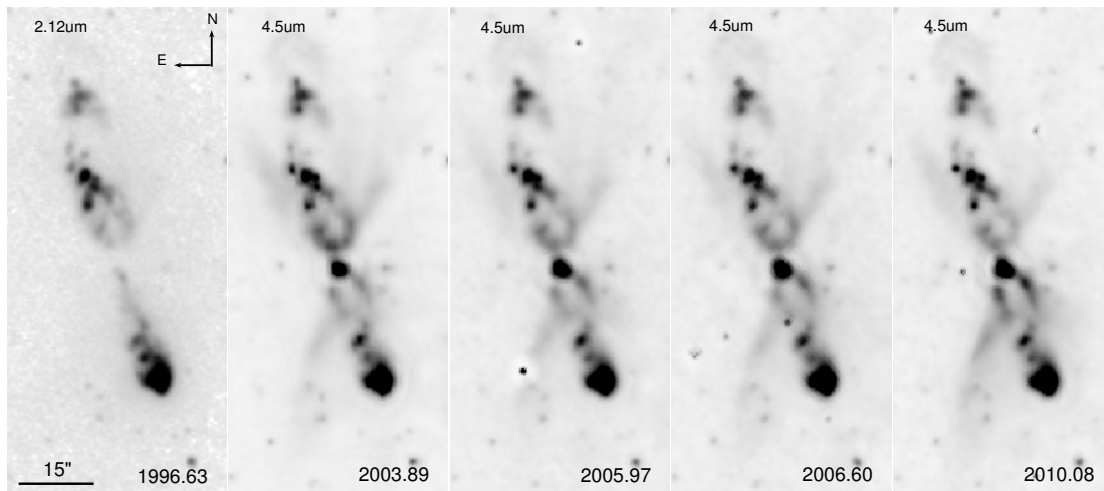


Figure 2. The other 5 epochs of Cep E data used to determine the NIR/midIR proper motion of its knots, including the 1996.63 $2.12 \mu\text{m}$ ground based image (first frame from left to right), plus the other 4 epochs of the AWAIC HiRES IRAC images at $4.5 \mu\text{m}$, after 60 iterations (see Table 1).

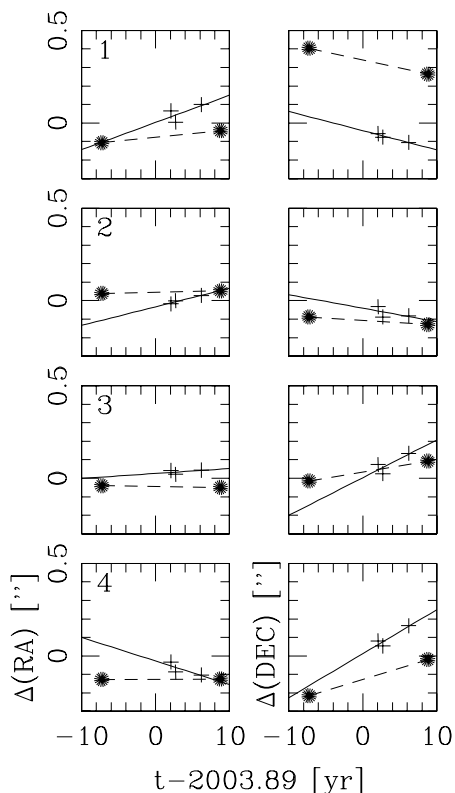


Figure 3. The offsets in arcseconds in RA and DEC between the 5 epochs of Cep E as measured in 4 different boxes; two each for the North and South lobes of the outflow (see Figure 4). The symbols correspond to the $2.12 \mu\text{m}$ (stars) and $4.5 \mu\text{m}$ (plus signs) data, respectively.

structures, see Figure 4) show substantial N-S motions, while the “cavity tips” (boxes 2 and 3) have considerably lower proper motions. We have then carried out linear fits to the time dependencies of the RA and DEC offsets of our four boxes, from which we obtain the proper motions (and their associated errors) given in Tables 2 ($2.12 \mu\text{m}$) & 3 ($4.5 \mu\text{m}$).

The proper motions obtained from the $2.12 \mu\text{m}$ and IRAC $4.5 \mu\text{m}$ do show similar trends and are within a fac-

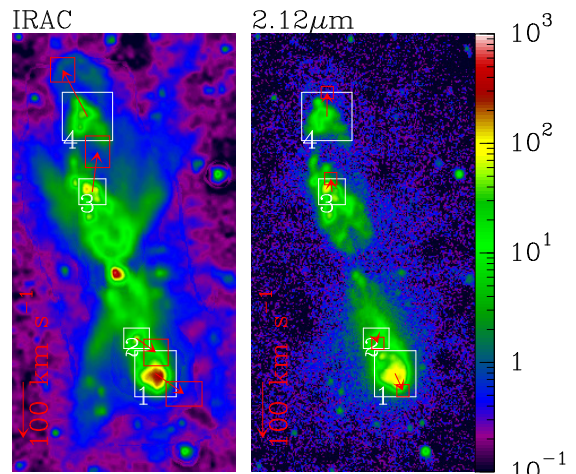


Figure 4. The tangential velocities of the H_2 emission as detected in IRAC $4.5 \mu\text{m}$ (left) and $2.12 \mu\text{m}$ (right) in the four boxes used in this study (see Table 2 & 3).

tor two (Table 2). One interesting thing to notice is that by placing all displacements on the same frame of reference, one can measure also a shift between the positions of the vibrational ($2.12 \mu\text{m}$) and rotational ($4.5 \mu\text{m}$) H_2 emission in the outflow. These are of the order of $0.25''$ – $0.30''$, certainly larger than the $0.05''$ – $0.10''$ positional uncertainty of the selected regions. The H_2 proper motions show evidence, for first time, that both the vibrational and rotational H_2 can share the same kinematics within an outflow; and furthermore, that the vibrational and rotational H_2 gas do trace slightly different regions within the outflow. Although this last statement may seem obvious within the now classical scenario of the acceleration of a molecular outflow, where the atomic/ionic supersonic flow drags and/or excites the surrounding molecular gas (see e.g. Raga et al. 1995), this is (to our knowledge) one of the first observational evidence that this is the case for the different components of the H_2 gas. Recall that spectroscopically we do have some good examples where both near-IR and mid-IR H_2 emission lines have been observed simultaneously in an outflows. Perhaps one of best examples is that of OMC-1 (Rosenthal,

Bertoldi & Drapatz 2000) where the Short Wavelength Spectrometer (SWS) detected 56 H_2 transitions within its 2.5 to 45 μm spectral range, and where the rotational emission was tracing a H_2 gas with an excitation temperature of 600 K, while the vibrational emission was tracing one at 3200 K. In OMC-1 it was possible to explain the bulk of the emission with collisional excitation produced by a combination of C-type and J-type shocks (Rosenthal, Bertoldi & Drapatz 2000). In Cep E, the spectroscopic evidence (Moro-Martin et al. 2001) also suggest a mixture of excitations to explain the optical and near/mid/far IR observations.

The resulting tangential velocities are shown (together with their error boxes) in Figure 4. Because of the multiple epochs, the motions seem to be better defined at 4.5 μm than at 2.12 μm . At 4.5 μm , the bow-like structures show proper motions of 94 km s^{-1} (Southern bow, box 1) and 63 km s^{-1} (Northern bow, box 4) directed approximately away from the outflow source. The Southern cavity tip (box 2) has essentially zero proper motion in the X-axis, and if this is the case it follows the flow of the bowshock but at steeper angle. The Northern cavity tip (box 3) shows a proper motion of 44 km s^{-1} at an angle of $\sim 60^\circ$ from the outflow direction (see Figure 4). This proper motion measurement might be affected by significant intensity variations of the cavity emission during the observed time period (see Figure 2).

4. NUMERICAL SIMULATIONS

In one of the first studies of the H_2 NIR emission in Cep E (Eisloffel et al. 1996) the authors suggested that the “wiggles and sideways positional offsets” were due to precession, with a relatively small precession angle of 4° . In the same study they noticed the presence of a couple of H_2 knots emanating westward from the central source and nearly perpendicular to the main Cep E outflow (Eisloffel et al. 1996, Figure 3), suggesting a very close-by second protostar, and therefore, a possible mechanism to drive the precession. To further test this hypothesis and compare with the kinematical behavior of the H_2 gas derived from the proper motion measurements, we present in this section some relatively simple 3D hydrodynamical simulations. The YGUAZU-A code (Raga et al. 2000, Raga et al. 2003) was selected for this simulation. The code, in a nutshell, uses a binary adaptive grid and integrates the gas-dynamic equations with a second-order accurate scheme (in time and space) using a flux-vector splitting method (van Leer 1982). The code has been used over a decade to simulate the gas dynamical processes that take place in several astrophysical scenarios including YSO outflows (e.g. Raga et al. 2004), proto-planetary nebulae (Velázquez et al. 2011), supernova explosions (Velázquez et al. 2004), photodissociation regions (Reyes-Iturbide et al. 2009), photoevaporating clumps (Raga, Steffen & Gonzalez 2005), and MIRA’s turbulent wake (Raga et al. 2008) among other. In this version of the code we include a H_2 gas component, although we cannot distinguish between its vibrational/rotational excitation.

The goal of the simulation is not to model in detail Cep E, but to show that the observed proper motions can indeed be explained when taking into account precession. Because of the relatively small dynamical age of the Cep E outflow (~ 3000 yr), we set the initial condi-

tions of the model as that of a jet emerging from a compact dense cold core with the simplifying assumption that it is in thermal balance with the surrounding medium ($n_{core} = 1000 \text{ cm}^{-3}$, $T_{core} = 1 \text{ K}$, $n_{ISM} = 10 \text{ cm}^{-3}$, $T_{ISM} = 10^3 \text{ K}$). Based on our previous simulations (Raga et al. 2004), we assume that the jet has an initial radius of $1.5 \times 10^{16} \text{ cm}$, a temperature of 1000 K and a velocity of 200 km s^{-1} , with a time dependent velocity variation (“pulses”) of a 50% over a 60 yr period. The jet is set to precess on a 10° angle with respect to its cylindrical symmetry axis over a 1200 yr period. Since we are interested on the bulk motion of the gas to compare with what is observed in the proper motions, we have chosen a medium resolution computational grid of $128 \times 128 \times 256$ cells set to a scale of $(X,Y,Z) = (5,5,10) \times 10^{17} \text{ cm}$, respectively. The time resolution is set to 200 yr per step, so once the jet plunges through the core, it takes 15 to 20 frames to reach a dynamical age close to that of Cep E.

The results of the simulation for the H_2 number density are shown for five time steps starting at the moment when the jet finally breaks free from the dense core (Figure 5; step 45). In all cases we present the XZ projection, i.e. perpendicular and along the flow. In the H_2 number density one already can see that the initial effect of precession has been to widen the path of the flow and the creation of two different density maxima upstream. At about 2000–3000 yr later (steps 56 and 59), the maxima have nearly merged and the flow is compact and asymmetric.

In an effort to better compare the numerical model with the observations we have integrated in the 3D grid the H_2 emission along the line of sight and projected it on a 30° angle. We have taken the difference in the projected emission for models 56 and 59 (i.e. a 600 yr interval), to mimic as much as possible the proper motion measurements. The result (Figure 6) shows at least four “knots” with tangential velocities ranging from 10 to 50 km s^{-1} on slightly different directions, although the bulk of the motion is away from the center of the grid. A 50 km s^{-1} tangential velocity is certainly consistent with the value of $\sim 62 \text{ km s}^{-1}$ of the North lobe, that plunges deeper into the cloud, and is a bit smaller than the 94 km s^{-1} value of the South lobe, where one detects at optical wavelengths HH 377, i.e the observed proper motions seem to reflect the difference in physical environment between the two lobes.

5. SUMMARY

We have derived proper motions based on six IR images of the Cep E outflow. Two ground based images obtained in 1996 and 2012 in $H_2 v=1-0$ at 2.12 μm , plus another four obtained at 4.5 μm with the Spitzer’s IRAC camera over the 2003–2010 time period.

We have defined four cross-correlation boxes that included the more compact emission structures. Two boxes for the tips of the two-ridged cavities (boxes 2 and 3, respectively, in Figures 3 & 4) and those for the Northern and Southern bowshocks (boxes 1 & 4, respectively). The proper motion of the tip of ridges is complex in both the rotational and vibrational emission and and it may reflect time dependent variation in their illumination or excitation. On the other hand, the proper motions of the main

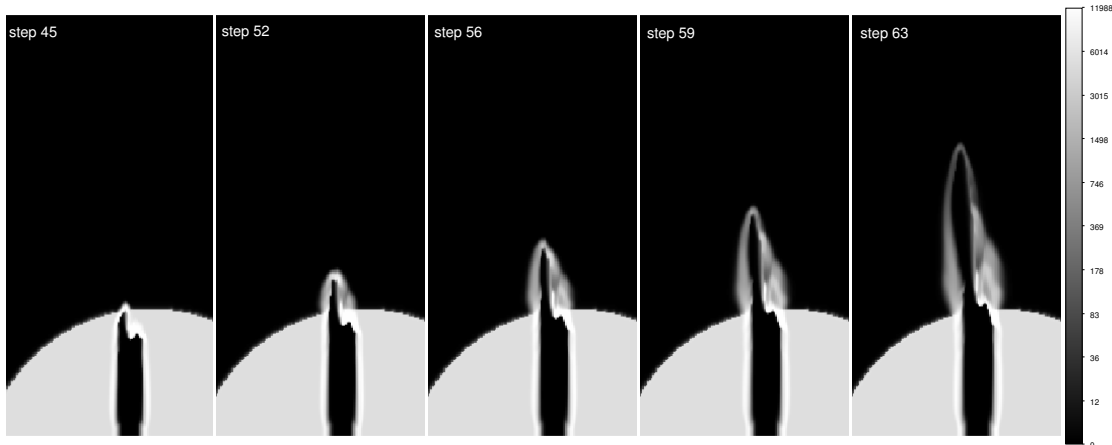


Figure 5. The H₂ number density [from 0 (black) to $1.2 \times 10^3 \text{ cm}^{-3}$ (white)] for a precessing jet emerging from a cold core to simulate the Cep E outflow.

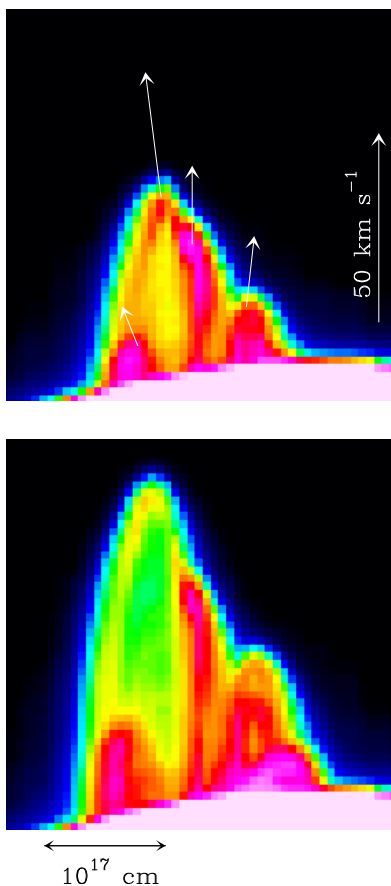


Figure 6. Tangential velocities of the H₂ gas as projected on the sky and based on models 56 and 59 (top). The overall morphology resembles that of the North lobe of Cep E (bottom).

bowshocks are well defined; they are moving away from the central source along the symmetry axis with tangential velocities of 62.6 ± 29.5 and $94.0 \pm 26.5 \text{ km s}^{-1}$, respectively. The Southern bowshock is detected also at optical wavelengths and is known as HH 377, and its proper motion has been measured (Noriega-Crespo & Garnavich 2001) rendering a tangential velocity of $(107 \pm 14) \text{ km s}^{-1}$, directed approximately along the outflow axis. This motion is roughly consistent with the proper motion that we have obtained for the IR emission of this object. The

proper motions based on the $2.12 \mu\text{m}$ emission are about a factor two smaller than those in the mid-IR. With a time baseline of $\sim 16 \text{ yr}$ and an angular resolution of $\sim 1''$, a priori one does not have any reason to believe that this difference in magnitude is not real. If this is the case, then the offset between the vibrational and rotational H₂ emission, plus the difference in velocity, suggests a different physical 'layer' in the outflow where the vibrational H₂ gas is excited. That not all the molecular tracers originate in the same place in young stellar outflows, including Cep E, has been nicely illustrated by a recent study of water using *Herschel* Space Telescope observations (Tafalla et al. 2013). For Cep E, for instance, the H₂O ($2_{12} - 1_{01}$ 1670 GHz), CO ($J = 2-1$) and H₂ emission (from IRAC $3.6 \mu\text{m}$ channel) at the same angular resolution ($13''$), show a very different spatial distribution along the flow axis (Tafalla et al. 2013, Figure 4). In this case, the CO emission peaks closer to the source, while the H₂O and H₂ share the same distribution farther away from the source. This means that gas at a temperature of tens of Kelvins (from CO) resides at a different place than gas at hundreds of Kelvins (from H₂O and H₂). A similar process could be taking place in our case, where the H₂ rotational emission, as measured by IRAC at $4.5 \mu\text{m}$ (i.e. S(11), S(10) & S(9) lines) is tracing a higher kinetic temperature than the vibrational H₂ traced by the $2.12 \mu\text{m}$ emission (see e.g. Giannini et al. 2011, Neufeld et al. 2009) and it is moving at a higher velocity as well.

As mentioned in the Introduction, the observed emission at $4.5 \mu\text{m}$ from young stellar outflows is likely produced by three rotational transitions of H₂. In the case of Cep E, in particular, one expects only a small contribution from the dust continuum emission at these wavelengths based on what is observed spectroscopically at $5 \mu\text{m}$ in its North lobe (Noriega-Crespo et al. 2004b). Thus the infrared proper motions imply that the molecular Hydrogen gas in Cep E is moving supersonically, just like its atomic/ionic counterpart. That the H₂ gas can have large tangential velocities in young stellar outflows was first noticed in the HH 1-2 system (Noriega-Crespo et al. 1997b), where velocities as high as 400 km s^{-1} , comparable to those from the optical tracers, were measured. Large H₂ flow velocities derived from proper motion measurements are now certainly not uncommon in young

stellar outflows (Chrysostomou et al. 2000; Caratti o Garatti et al. 2009; Zhang et al. 2013),

The large tangential velocities of H_2 gas in Cep E or other young stellar outflow are somewhat of a puzzle. In these outflows, the bulk of the H_2 emission arises from collisional excitation due to shocks, although turbulence and entrainment may also play a role (Reipurth & Bally 2001; Noriega-Crespo 1997a; Raga et al. 2003). The shocks exciting the H_2 gas cannot be that strong because otherwise the molecule dissociates, and this occurs at shock velocities of $\sim 45 \text{ km s}^{-1}$ even in the presence of strong magnetic ($\sim 50 \mu\text{G}$) fields (Lepp & Shull 1983; Draine, Roberge & Dalgarno 1983). There are, however, models of the H_2 emission where higher shock velocities are possible (Le Bourlot et al. 2002). In these models, if one allows for an initial magnetic field $\geq 100 \mu\text{G}$, i.e. about a factor 5 or 10 larger than what is measure at densities of $10^2\text{--}10^3 \text{ cm}^{-3}$ in interstellar clouds (Crutcher et al. 2010), then it is possible to reach shock velocities as high as $70\text{--}80 \text{ km s}^{-1}$. That magnetic fields does play a major role in outflows is nicely capture by the work on the survival of CO and H_2 in magnetized protostellar disk winds by Panoglou et al. (2012). Although this work concentrates on scales closer to the launching of the flows (i.e. with a few au), emphasizes the role of chemistry for the formation and survival of the molecules. At larger scales, however, “internal shock waves” (either J or C-shocks) that arise as a result of time variability or instabilities of the flow, will control which molecules are destroyed or reformed (Panoglou et al. 2012).

Since the bright condensations or knots that one observes in the collimated outflows are ejected from the driving source nearly “ballistically” (see e.g. Raga 1993), then the survival of the H_2 gas needs to be fine tuned in terms of the relative velocities of the ejected gas. The relatively simple 3D hydrodynamical numerical simulations to model Cep E presented here (i.e. without including magnetic fields or a chemistry network), although limited, do show tangential velocities as high as $\sim 50 \text{ km s}^{-1}$, i.e. near the threshold of H_2 dissociation if the gas is being collisionally excited. Higher shock velocities, like what we have measured in Cep E, require strong magnetic fields for the H_2 molecules to survive (Panoglou et al. 2012), or a very efficient reformation mechanism (Raga, Williams & Lim 2005)

The authors thank the referees and editors for their careful reading of the manuscript and their valuable suggestions. In particular the realization that rotational H_2 can trace higher kinetic temperatures than the vibrational ones. This research is based in part on observations made with the *Spitzer Space Telescope* (NASA contract 1407) and has made use of the NASA/IPAC Infrared Science Archive, both are operated by the Jet Propulsion Laboratory, California Institute of Technology, under contract with the National Aeronautics and Space Administration (NASA).

REFERENCES

Ayala, S., Noriega-Crespo, A., Garnavich, P. M., Curiel, S., et al. 2000, *AJ*, 120, 909
 Bally, J. 2009 in *Protostellar Jets in Context*, by Kanaris Tsinganos, Tom Ray, Matthias Stute. *Astrophysics and Space Science Proceedings Series*. pp.11-20

Bally, J. Reipurth & Davis 2007 in *Protostars and Planets V*, B. Reipurth, D. Jewitt, and K. Keil (eds.), University of Arizona Press, Tucson, p.215-230
 Boulanger, F., Lorente, R., Miville Deschênes, M. A., Abergel, A., et al. 2005, *A&A*, 436, 1151
 Chrysostomou, A., Hobson, J., Davis, C. J., Smith, M. D. & Berndsen, A. 2000, *MNRAS*, 314, 229
 Caratti o Garatti, A., Eisloffel, J., Froebrich, D. et al. 2009, *A&A*, 502, 579
 Caratti o Garatti, A. & Eisloffel, J. 2009 in *Protostellar Jets in Context*, by Kanaris Tsinganos, Tom Ray, Matthias Stute. *Astrophysics and Space Science Proceedings Series*. pp.329-339
 Crutcher, R.M., Wandelt, B., Heiles, C., Falgarone, E. & Troland, T.H. 2010, *ApJ*, 725, 466
 Draine, B. T., Roberge, W. G., & Dalgarno, A. 1983, *ApJ*, 264, 485
 Eisloffel, J., Smith, M. D., Davis, C. J & Ray, T.P. 1996, *AJ*, 112, 2086
 Fazio, G. et al. 2004, *ApJS*, 154, 10
 Gómez-Ruiz, A. I., Gusdorf, A., Leurini, S., Codella, C. et al. 2012, *A&A*, 542, 9
 Hatchell, J., Fuller, G. A. & Ladd, E. F. 1999, *A&A*, 346, 278
 Hartigan, P., Frank, A., Foster, J.M. et al. 2011, *ApJ*, 736, 29
 Herbig, G. H. & Jones, B.F. 1981, *AJ*, 86, 123
 Herbig, G. H. & Jones, B. F. 1983, *AJ*, 88, 1040
 Jarrett, T. H., Masci, F., Tsai, C. W., Petty, S. et al. 2012, *AJ*, 144, 68
 Ladd, E. F. & Hodapp, K.-W. 1997, *ApJ*, 474, 749
 Le Bourlot, J., Pineau des Forets, G., Flower, D.R. & Cabrit, S. 2002, *MNRAS*, 332, 985
 Lefloch, B., Eisloffel, J., Lazareff, B. 1996, *A&A*, 313, 17
 Lefloch, B., Cernicharo, J., Pacheco, S., Ceccarelli, C. 2011, *A&A*, 527, 3
 Lepp, S. & Shull, J. M. 1983, *ApJ*, 270, 578
 Looney, L. W., Tobin, J. J., Kwon, W. 2007, *ApJ*, 670, 131
 Masci, F. J. & Fowler, J. W. 2009, *ASPC*, 411, 67
 McKee, C.F. & Ostriker, E.C. 2007, *ARAA*, 45, 565
 Moro-Martín, A., Noriega-Crespo, A., Molinari, S., Testi, L. et al. 2001, *ApJ*, 555, 146
 Neufeld, D. A., Nisini, B., Giannini, T. et al. 2009, *ApJ*, 706, 170
 Noriega-Crespo, A. 1997 in “Herbig-Haro Flows and the Birth of Stars; IAU Symposium No. 182”, Ed. by B. Reipurth & C. Bertout. Kluwer Academic Publishers, 1997, p. 103-110.
 Noriega-Crespo, A., Garnavich, P. M., Curiel, S. Raga, A. C. & Ayala, S. 1997, *ApJ*, 486, 55
 Noriega-Crespo, A., Garnavich, P. M. & Molinari, S. 1998, *AJ*, 116, 1288
 Noriega-Crespo, A. & Garnavich, P. 2001, *AJ*, 122, 331
 Noriega-Crespo, A. et al. 2004a, *ApJS*, 154, 352
 Noriega-Crespo, A. et al. 2004b, *ApJS*, 154, 402
 Noriega-Crespo, A. & Raga, A.C. 2012, *ApJ*, 750, 101
 Panoglou, D., Cabrit, S., Pineau Des Fortes et al. 2012, *A&A*, 538, 2
 Padoan, P., Juvela, M., Kritsuk, A., & Norman, M. L. 2009, *ApJ*, 707, 153
 Plunkett, A., Arce, H. G., Corder, S. A. et al. 2013, *ApJ*, 774, 22
 Quillen, A. et al. 2005, *ApJ*, 632, 941
 Raga, A. C. 1993, *Ap&SS*, 208, 163
 Raga, A. C., Taylor, S. D., Cabrit, S., & Biro, S. 1995, *A&A*, 296, 833
 Raga, A. C., Bhm, K.-H. & Raymond, J. 2000, *AJ*, 120, 909
 Raga, A. C., Velázquez, P. F., de Gouveia dal Pino, E. M., Noriega-Crespo, A. & Mininni, P. 2003, *RMxAC*, 15, 115
 Raga, A. C., Noriega-Crespo, A., González, R. F. & Velázquez, P. F. 2004, *ApJS*, 154, 346
 Raga, A.C., Steffen, W., & González, R.F. 2005, *RMxAA*, 41, 443
 Raga, A. C., Williams, D. A. & Lim, A. J. 2005, *RMxAA*, 41, 137
 Raga, A.C., Cantó, J., De Colle, F. et al. 2008, *ApJ*, 680, 45
 Raga, A.C., Reipurth, B., Canto, J., Sierra-Flores, M.-M. & Guzman, M.V. 2011, *RMxAA*, 47, 425
 Raga, A. C. Noriega-Crespo, A., Lora, V., Stapelfeldt, K. R. & Carey, S. 2011 *ApJ*, 730, 17
 Raga, A. C., Noriega-Crespo, A., Rodríguez-González, A., Lora, V., Stapelfeldt, K. R. & Carey, S. J. 2012, *ApJ*, 748, 103
 Raga, A.C., Noriega-Crespo, A., Carey, S. J. & Arce, H. G. 2013, *AJ*, 145, 28 (Paper I)
 Raymond, J. C. 1979, *ApJS*, 39, 1
 Reipurth, B. & Bally, J. 2001, *ARAA*, 39, 403
 Reipurth, B., Bally, J., Colin, A. et al. 2013, *AJ*, 146, 118
 Reyes-Iturbide, I., Velázquez, P.F., Rosado, M. et al. 2009, *MNRAS*, 394, 1009
 Rodríguez, L.F. 2011 *IAUS* 27, 376
 Rosenthal, D., Bertoldi, F. & Drapatz, S. 2000, *A&A*, 356, 705
 Tafalla, M., Liseau, R., Nisini, B. et al. 2013, *A&A*, 551, 116
 Tobin, J. J., Looney, L. W., Mundy, L. G., Kwon, W., Hamidouche, M. 2007, *ApJ*, 659, 1404
 Ybarra, J. E., Lada, E. A. 2009, *ApJ*, 695, 120

- van Leer, B. 1982 in Numerical Methods in Fluid Dynamics, ed. E. Krause (Lecture Notes in Physics, Vol. 170; Berlin: Springer), 507
- Velázquez, P.E., Martinell, J.J., Raga, A.C. & Giacani, E.B. 2004, ApJ, 601, 885
- Velázquez, P.E., Wolfgang, S., Raga, A.C. et al. 2011, ApJ, 734, 57
- Velusamy, T., Langer, W. D. & Marsh, K. A. 2007, ApJ, 668, 159
- Velusamy, T., Marsh, K. A., Beichman, C. A., Backus, C. R., & Thompson, T. J. 2008, AJ, 136, 197
- Velusamy, T., Langer, W. D., Kumar, M. S. N. & Grave, J. M. C. 2011, ApJ, 741, 60
- Velusamy, T., Langer, W.D. & Thompson, T. 2014, ApJ, 783, 6
- Wilson, J.C. et al. 2003, SPIE, 4841, 50
- Zhang, M., Brander, W., Wang, H. et al. 2013, A&A, 553, 41